International Journal of Heat and Mass Transfer 52 (2009) 5013–5019

Contents lists available at ScienceDirect

International Journal of Heat and Mass Transfer

journal homepage: www.elsevier.com/locate/ijhmt

Diffusion and reaction controlled dissolution of oxygen microbubbles in blood

Magnus Fischer, Igor Zinovik, Dimos Poulikakos *

Laboratory of Thermodynamics in Emerging Technologies, Institute of Energy Technology, Department of Mechanical and Process Engineering, ETH Zurich, 8092 Zurich, Switzerland

ARTICLE INFO

Article history:
Received 13 November 2008
Received in revised form 7 April 2009
Available online 24 June 2009

Keywords:
Facilitated diffusion
Microbubbles
Moving interface
Blood saturation
Oxygen uptake

ABSTRACT

A model for the dissolution of a bubble in blood is presented in this paper. The gas inside the bubble is oxygen and the collapse of the bubble is controlled by the diffusion of the gas from the bubble surface into the surrounding blood. The diffusion is facilitated by the oxygen uptake reaction between the dissolved gas and the hemoglobin, which is described using the Hill saturation curve. The model consists of a system of coupled differential equations describing the related mass transfer physics in an expanding computational domain, which follows the moving interface between the shrinking bubble and the surrounding blood. The main findings regarding the important collapse time of microbubbles in blood indicate that this time may vary from 10 s to 2 or 3 h depending on the size of the bubbles and on the parameters which specify the blood conditions.

1. Introduction

Gas bubbles can form in the blood stream as a result of the specific physiological conditions or therapeutic and surgical interventions. Examples of physiological conditions include the decompression sickness of divers and the generation of microbubbles by mechanical prosthetic heart valves. Gas bubbles may also appear during non-invasive lithotripter procedures to eliminate kidney stones. Micron-size bubbles are often used as ultrasound contrast agents in medical imaging. Microbubbles originated in a cardiopulmonary bypass or in other extracorporeal tubing can be infused into blood circulation during invasive procedures or hemodialysis. A classification of gas embolism, procedures and events generating microbubbles as well as the clinical consequences of circulating microbubbles in blood is presented in [1,2]. It is known that the presence of a large amount of gas in the blood circulation results in serious medical complications. The uncertainty about the fate of the bubbles stipulates extensive experimental and modeling efforts to develop methods for the control and management of bubbles in blood circulation [2].

A number of models of dissolving bubbles in a stream of fluid have been developed to support simulations for different industrial processes [3–8]. If the chemical reactions are neglected, the models rely on the Navier–Stokes equations [9–14]. In blood flow, the simulations describe the bubbles in unsteady flow conditions induced by ultrasound oscillations [11–13] or cavitation [14]. These simulations assume spherical symmetry and adopt solutions of the Rayleigh–Plesset equation with its extension which models the non-Newtonian behavior of blood [11].

If the dynamics of the bubble is induced by the diffusion of gas from the bubble into blood, the simulations utilize the Epstein–Plesset model suggested in [15]. An extension of the Epstein–Plesset model for the simulation of multi-component gas bubbles in blood is suggested in [16]. If the blood pressure changes rapidly, the Epstein–Plesset solution is applied together with the Rayleigh–Plesset equation, which describes the pressure field around the bubble [17,18].

If the bubble contains oxygen, the diffusion of the gas into blood is accompanied by the chemical reaction of oxygen with hemoglobin. The hemoglobin combines reversibly with molecular oxygen and forms oxyhemoglobin. The reaction of oxygen uptake is of crucial importance for oxygen transport in blood circulation. It has been extensively investigated since the beginning of the previous century and remains to be the focus of ongoing biochemical studies. An extensive review of the existing literature devoted to the chemical reactions between oxygen and hemoglobin is out of scope of this work. In problems dealing with dissolving bubbles, the reaction of oxygen with hemoglobin is simulated as a simple binding process with constants defining the kinetic rates of forward and backward reactions [19,20].

An example of modeling the oxygen uptake as a first-order chemical reaction is shown in [21]. The calculated lifetime of the bubbles is of the same order of magnitude as the collapse time which was observed in the experiments [22]. The same first-order reaction model is also applied to the analysis of a hemiellipsoidal bubble in a blood flow [23,24]. The results of the experiments show that the model underestimates the lifetime of the bubbles in blood. The deviation is attributed to the over-simplified model of the oxygen uptake reaction. Experimental measurements of oxygen transfer kinetics in blood [25–29] show that the forward and reverse kinetic rate constants are very sensitive to the chemical reaction

* Corresponding author. Tel.: +41 44 63 22039; fax: +41 44 63 21176.
E-mail address: dimos.poulikakos@ethz.ch (D. Poulikakos).

0017-9310/$ - see front matter © 2009 Elsevier Ltd. All rights reserved.
doi:10.1016/j.ijheatmasstransfer.2009.05.013

Nomenclature

Latin symbols

C_b	mass fraction of bound oxygen (–)
C_d	mass fraction of dissolved oxygen (–)
C_t	mass fraction of oxygen in blood (–)
c	hemoglobin binding capacity (ml O_2)(ml blood)$^{-1}$
D	diffusivity coefficient (m^2 s^{-1})
D_F	facilitated diffusivity coefficient (m^2 s^{-1})
j	mass flux density (kg m^{-2} s^{-1})
L_D	length of the computational domain (m)
n	parameter of Hill's equation (–)
P_{50}	parameter of Hill's equation (mmHg)
P_{O_2}	partial pressure of dissolved oxygen (mmHg)
P_R	pressure inside the bubble (mmHg)
R,X	bubble radius (m) (–)
r,x	radial coordinate (m) (–)
S	oxygen saturation (–)
t	time (s)
T_c	collapse time (s)
V_{O_2}	volumetric content of oxygen in blood (–)

Greek symbols

α	solubility of oxygen (ml O_2)(ml blood)$^{-1}$(mmHg)$^{-1}$
δ	domain extension (–)
η	radial Landau coordinate (–)
λ	slope of the saturation curve (–)
ρ_b	density of blood (kg m^{-3})
ρ_{STP}	density of oxygen under standard conditions (kg m^{-3})
τ	dimensionless time (–)
φ	normalized mass fraction (–)

parameters of the hemoglobin molecules, the concentration of erythrocytes blood and to other physiological conditions.

The lifetime of bubbles in blood is usually much smaller than the half-time of oxygen uptake. The size of bubbles circulating in blood flow lies within the range of 1–250 μm [17,18,30,31] and the dissolution times of such bubbles may vary from 1 to 600 s. If the characteristic time of a process in question differs significantly from the half-time of the reaction of oxygen uptake, the binding of oxygen can be treated as an instant reaction thus avoiding the uncertainty that comes from the choice of the kinetic constants. The separation of slow and fast dynamics of a problem is widely used in chemical and biochemical engineering [32–34]. The results shown in [35–37] indicate that this approach accurately predicts the concentration of oxygen in the blood–gas exchange devices [35–37].

The objective of the present work is to support the development of medical procedures and biomedical devices requiring the understanding of the physics and the control of the dynamics of microbubbles in blood circulation. The goal of the model herein is to analyze the dynamics of the diffusion-induced collapse of bubbles of oxygen in blood. The simulations employ a "facilitated" diffusion model. Unlike earlier simulations of bubbles in blood, the present model accounts for oxygen–hemoglobin interaction which has been shown to be important in experiments. The results of the simulations provide us with an insight into the oxygen transport in blood, caused by the dissolution of microbubbles.

2. Governing equations

In the presented model, the bubble is assumed to be spherical and surrounded by blood at rest. Inertial and temperature effects within the bubble and in the blood are neglected due to the relatively small size of the simulated bubbles. The gas in the bubble is oxygen, which is modeled as an inviscid ideal gas. The pressure within the bubble is assumed to be spatially uniform. Earlier simulations [15,21] of microbubbles dissolving in water and in blood indicate that the effect of surface tension decreases the collapse time by less than 3%. Therefore, the surface tension is not modeled in the present simulations, and it is assumed that the gas pressure within the bubble does not change over time. The last assumption implies that the dynamics of the surface of the bubble is controlled solely by the diffusion of gas through the interface into the blood. To this end, the model is limited to cases where dissolved gases other than oxygen do not significantly affect the dynamics of the bubble collapse.

The oxygen in the blood includes the physically dissolved oxygen and the hemoglobin bound oxygen inside red blood cells. The mass diffusion of the dissolved oxygen is governed by Fick's law with a constant diffusivity coefficient D. It is also assumed that the concentration of the dissolved oxygen at the gas–blood interface is governed by Henry's law with a constant solubility α. The hemoglobin bound oxygen is assumed to be in equilibrium with the dissolved oxygen. The degree of oxygen bound to hemoglobin in the blood is expressed using the Hill equation as the oxygen saturation S [19]:

$$S(P_{O_2}) = \frac{(P_{O_2}/P_{50})^n}{1 + (P_{O_2}/P_{50})^n}, \tag{1}$$

where P_{O_2} is the partial pressure of the dissolved oxygen. Both P_{50} and n are constant parameters that depend on the physiological conditions of the blood and are usually derived from fitting experimental data. The total volumetric content of oxygen in blood V_{O_2} is usually calculated as a sum of the concentrations of free physically dissolved oxygen and oxygen bound to hemoglobin as follows:

$$V_{O2} = \alpha P_{O2} + cS, \tag{2}$$

where c = 0.166 (ml O_2)(ml blood)$^{-1}$ and α = 0.3 (ml O_2)(ml blood)$^{-1}$ (mmHg)$^{-1}$ are the hemoglobin binding capacity and the physical solubility of oxygen, respectively [37]. The density of oxygen dissolved in blood is much less than the density of blood thus the total mass fraction C_t of oxygen in blood can be calculated as follows:

$$C_t = \frac{\rho_{STP}}{\rho_b} V_{O2} = \frac{\rho_{STP}}{\rho_b}(\alpha P_{O2} + cS) = C_d + C_b, \tag{3}$$

where ρ_{STP} is the density of oxygen under standard conditions of atmospheric pressure and temperature of 273 K, ρ_b is the density of blood, and $C_d = (\rho_{STP}/\rho_b)\alpha P_{O2}$, $C_b = (\rho_{STP}/\rho_b)cS$ denote the mass fractions of dissolved and bound oxygen, respectively.

Under normal physiological conditions, the molecules of bound oxygen are attached to the hemoglobin of the red blood cells (RBC), which have a diameter of about 10 μm. The diffusivity coefficient of the cells in blood is much lower than the diffusivity of the molecular dissolved oxygen. Thus in a control volume of blood, the diffusive fluxes of bound oxygen can be neglected compared to the fluxes of dissolved oxygen. The diffusion equation for total mass fraction of oxygen in blood can be written as follows:

$$\frac{\partial C_t}{\partial t} = D\Delta C_d. \tag{4}$$

The substitution of (3) into (4) yields:

$$\frac{\partial C_d}{\partial t} + c\frac{\rho_{STP}}{\rho_b}\frac{\partial S}{\partial t} = D\Delta C_d. \tag{5}$$

If the saturation S defined by (1) is written as a function of the concentration of dissolved oxygen utilizing the Henry's law, Eq. (5) becomes:

$$\frac{\partial C_d}{\partial t} + c\frac{\rho_{STP}}{\rho_b}\frac{dS(C_d)}{dC_d}\frac{\partial C_d}{\partial t} = D\Delta C_d. \tag{6}$$

The mass balance of dissolved oxygen in a control volume of blood (6) can be rewritten as an equation with a facilitated diffusivity coefficient D_F:

$$\frac{\partial C_d}{\partial t} = D_F\Delta C_d, \tag{7}$$

where $D_F = D/(1+\lambda)$. The slope λ of the saturation curve is a function of the unknown mass fraction of the dissolved oxygen:

$$\lambda = c\frac{\rho_{STP}}{\rho_b}\frac{n}{C_{50}}\left(\frac{C_d}{C_{50}}\right)^{n-1}\Bigg/\left(1+\left(\frac{C_d}{C_{50}}\right)^{n}\right)^2. \tag{8}$$

The equation for the shrinkage rate of the dissolving bubble is derived from a mass balance of the gas bubble. The mass of oxygen inside the bubble changes due to the flux j of gas through the surface of the bubble:

$$\rho_{STP}\frac{d}{dt}\left(\frac{4}{3}\pi R^3\right) = -4\pi R^2 j, \tag{9}$$

where R is the radius of the bubble. This yields an expression of the velocity of the interface:

$$\frac{dR}{dt} = -\frac{j}{\rho_{STP}}. \tag{10}$$

The flux j at the bubble–blood interface is calculated as follows:

$$j = -\rho_b D\left(\frac{\partial C_d}{\partial r}\right)_R, \tag{11}$$

where the normal derivative is calculated at the bubble surface and the mass fraction C_d is obtained from the solution of the facilitated diffusion Eq. (7). A radius–time relation for the dissolving bubbles is found by solving Eqs. (7), (9), and (11) together with appropriate boundary and initial conditions.

It is worth pointing out that the flux calculation is based on the physical diffusivity coefficient while in the facilitated diffusion equation, the coefficient D_F depends on the concentration of oxygen in blood. In the mass balance Eq. (7), the facilitated diffusivity coefficient combines the mass flux caused by the physical diffusion and the mass sink ($-\partial C_b/\partial t$) due to the oxygen uptake reaction. Strictly, Eq. (7) is not the diffusion transport equation with a concentration-dependent diffusivity coefficient. On this account a problem-specific numerical algorithm should be developed for the solution of this equation.

Simulations of microbubbles in blood reported in the literature usually employ the Epstein–Plesset model, which assumes a decoupling of the facilitated diffusion and the bubble radius–time relation. In the Epstein–Plesset model, the gradient of the concentration of dissolved gas on the shrinking surface of the bubble is computed based on the solution of the diffusion problem with a prescribed non-moving boundary. This gradient is then substituted into the equation for the radius–time relation. Compared to Epstein–Plesset, the present simulations utilize a numerical solution of the coupled system (7)–(11) where the shrinking of the bubble induces a moving boundary problem for Eq. (7). The obtained solution of the coupled problem allows an analysis of the assumption of the Epstein–Plesset model for microbubbles dissolving in blood.

The finite difference method is applied to solve Eqs. (7) and (10) simultaneously. The detailed description of the development and application of the algorithm to a multi-component diffusion problem with spherical symmetry is shown elsewhere [38], and the following section outlines an adaptation of the algorithm to the problem of a bubble dissolving in blood.

3. Numerical solution

The facilitated diffusion equation is solved in the spherical coordinate system assuming spherical symmetry for the mass fraction distribution of the dissolved oxygen:

$$\frac{\partial C_d}{\partial t} = D_F\left[\frac{2}{r}\frac{\partial C_d}{\partial r} + \frac{\partial^2 C_d}{\partial r^2}\right], \tag{12}$$

where r is the radial coordinate. The following initial and boundary conditions are imposed at the outer boundary of the computational domain and at the bubble–liquid interface:

$$C_d(t=0) = C_0 \quad C_d(\infty, t) = C_0 \quad C_d(R,t) = C_R. \tag{13}$$

The mass balance equation for the gas in the bubble is written as follows:

$$\frac{dR}{dt} = \frac{\rho_b}{\rho_{STP}}\frac{D}{1+\lambda}\left(\frac{\partial C_d}{\partial r}\right)_R. \tag{14}$$

In order to develop an efficient numerical algorithm, the following non-dimensional concentration, time and radial coordinate are introduced:

$$\phi = \frac{C_d}{C_0} \quad \tau = \frac{Dt}{R_0^2} \quad x = \frac{r-R_0}{R_0}. \tag{15}$$

The solution of the moving boundary problem requires a second transformation of the variables which is carried out using coordinates introduced by Landau [39]. The Landau coordinates are:

$$\eta(x,\tau) = \frac{x - X(\tau)}{\delta(\tau)} = \frac{x - X(\tau)}{X_\infty - X(\tau)}, \tag{16}$$

where $X(\tau)$ is the moving non-dimensional position of the bubble–liquid interface and X_∞ is the fixed boundary of the computational domain. In the Landau variables, the facilitated diffusion equation is written as follows:

$$\frac{\partial \phi}{\partial \tau} = A\frac{\partial \phi}{\partial \eta} + B\frac{\partial^2 \phi}{\partial \eta^2}, \tag{17}$$

where the coefficients A and B are defined as:

$$A = \frac{1}{\delta}\left(\frac{2}{(1+\lambda)(1+\eta\delta+X)} + (1-\eta)\frac{dX}{d\tau}\right), \tag{18}$$

$$B = \frac{1}{1+\lambda}\frac{1}{\delta^2}. \tag{19}$$

The mass balance of the gas in the bubble takes the form:

$$\frac{dX}{d\tau} = \frac{1}{(1+\lambda)}\frac{C_0}{\delta}\frac{\rho_b}{\rho_{STP}}\left(\frac{\partial \phi}{\partial \eta}\right)_{\eta=0}. \tag{20}$$

A 2nd order central differencing scheme in space and an implicit Euler scheme for the temporal discretization are utilized. The discretized facilitated diffusion equation is written as follows:

$$\frac{\phi_i^{n+1} - \phi_i^n}{\Delta\tau} = A\frac{\phi_{i+1}^{n+1} - \phi_{i-1}^{n+1}}{2\Delta\eta} + B\frac{\phi_{i+1}^{n+1} - 2\phi_i^{n+1} + \phi_{i-1}^{n+1}}{(\Delta\eta)^2}. \tag{21}$$

The position of the interface is updated using a 1st order approximation:

$$X^{n+1} = X^n + \left(\frac{dX}{d\tau}\right)^{n+1} d\tau. \tag{22}$$

Accurate coupling of the interface velocity ($dX/d\tau$) and the gradient of the concentration at the interface is of crucial importance for the solution. Once the oxygen bubble at atmospheric pressure is introduced into blood, the concentration of oxygen at the blood–gas interface is one order of magnitude higher than the concentration of the dissolved oxygen. This high ratio causes a steep gradient of the concentration which in turn strongly affects the results of the computation of the radius–time relation and the collapse time. For this reason, a 3rd order discretization scheme [40] for the calculation of the concentration gradient was added to the original algorithm [38]. This insures an accurate approximation of the velocity of the interface:

$$\left(\frac{dX}{d\tau}\right) = \frac{1}{(1+\lambda)}\frac{\rho_b C_0}{\rho_{STP}}\frac{-\phi_3 + 6\phi_2 - 3\phi_1 - 2\phi_0}{6\delta\Delta\eta}. \quad (23)$$

In Eq. (23) φ_0 is the dimensionless concentration in a fictitious node, which is calculated utilizing the finite difference Eq. (21). Preliminary tests showed that if the value of interface velocity appearing in the coefficient A of Eq. (21) is computed using the value from the previous time step, the solution shows spurious oscillations towards the end of the shrinking process. In order to remedy this deficiency, the interface velocity is obtained solving a quadratic equation, which is derived from (21) and (23) at the boundary of the domain (see Appendix A for the details).

4. Results and discussion

The profiles of blood saturation around a bubble with initial radius $R = 100$ μm is shown in Fig. 1. The following set of model parameters is chosen for the base case simulation: the pressure of oxygen inside the bubble is specified to be 760 mmHg and the initial concentration of oxygen in blood equals 51 mmHg; the parameters of the Hill's equation are set to be $n = 2.7$ and $P_{50} = 28$ mmHg. The diffusivity is assumed to be $D = 1.8 \times ! 10^{-5}$ cm^2 s^{-1} [19]. In this case, neglecting the effect of surface tension is a reasonable approximation because the increase of pressure inside the bubble due to surface tension is comparable with the initial pressure when the radius is about 1 μm, i.e. the size of the bubble decreases by two orders of magnitude.

In Fig. 1a, the profiles are shown in the Landau coordinates in a fixed computational domain. The last curve corresponds to the saturation profile at the moment of the bubble collapse. The results indicate that the saturation front rapidly propagates into blood in the first 22 s, and then the velocity of the front drops by 3–4 times and slows down until the full dissolution of the bubble. The fast initial velocity of the oxygenation front is qualitatively similar to rapid oxygenation of a thin layer of blood adjacent to the bubble observed in the experiments [22]. The same set of profiles as in Fig. 1a is illustrated in Fig. 1b in physical coordinates where the left endpoint of the profile coincides with the instant position of the interface. As oxygen diffuses into blood, the surface is shrinking towards its center. The shrinking is slightly accelerated over time. At the moment of collapse, oxygen from the bubble diffuses into a blood volume which is bounded by a sphere with a radius about three times greater than the initial radius of the bubble.

The results of earlier experiments [22] are used to validate the model of bubble dissolution presented in this work. In the experiments, radius–time relations of oxygen bubbles dissolving in degassed blood are recorded for bubbles with radii from 200 to 300 μm. In Fig. 2, the experimental data is compared with the results of the simulations. The parameters of blood under the conditions of the tests in [22] are not reported. In the simulations, the value of diffusivity D has been chosen to serve as a fitting parameter, while the Hill's constants are assumed to be the same as for Fig. 1. The best fit has been found with $D = 0.7 \times 10^{-5}$ cm^2 s^{-1}. This value is in the lower part of the physiological range as reported in

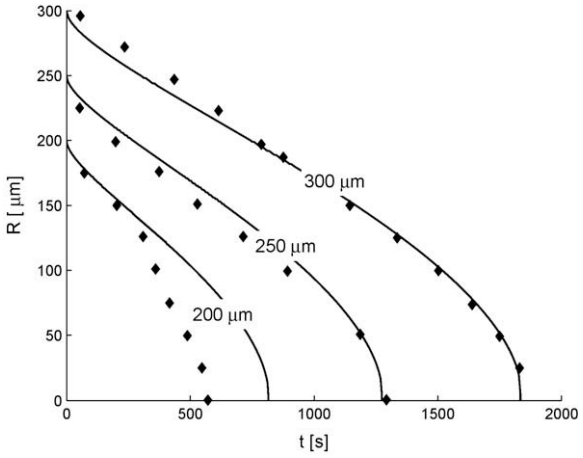

Fig. 2. Temporal evolution of the radius of dissolving bubbles in degassed blood. Experimental data are obtained from [24]. Numerical values: $D = 0.7 \times 10^{-5}$ cm^2 s^{-1}, $n = 2.7$, $P_0 = 51$ mmHg, pressure in bubble: $P_R = 760$ mmHg. The value of the initial radius is shown next to the corresponding curve.

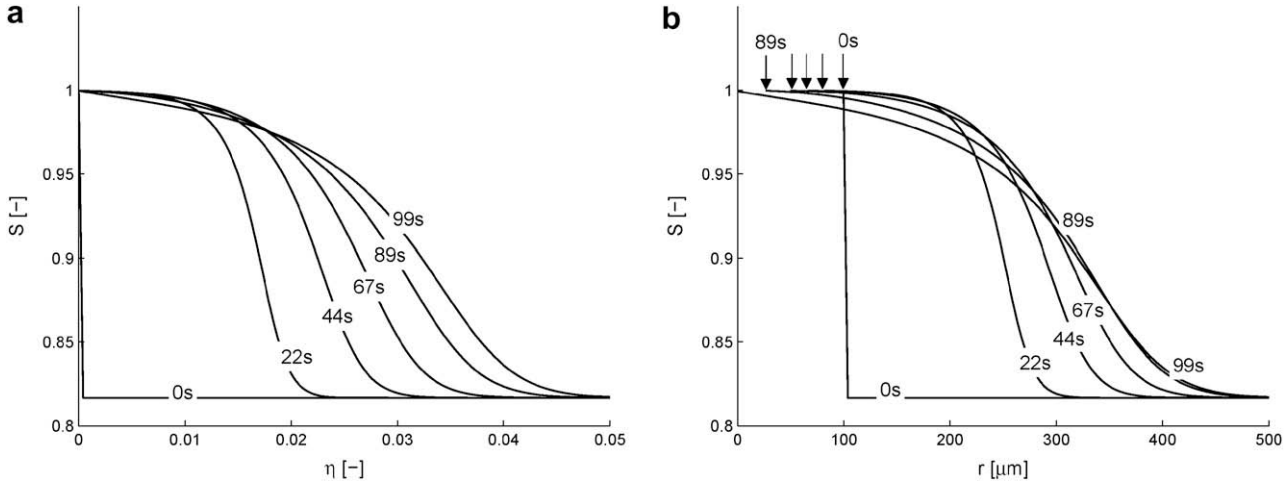

Fig. 1. Radial profiles of blood saturation around an oxygen bubble with initial radius of 100 μm, $D = 1.8 \times 10^{-5}$ cm^2 s^{-1}, $n = 2.7$, $P_0 = 51$ mmHg, $P_R = 760$ mmHg. On the left side the profiles are shown in fixed Landau coordinates (a) whereas the right figure (b) depicts the profile in physical coordinates.

[24]. The results of the simulations deviate less than 10% from the data for the bubbles with radii 250 and 300 μm. For the smaller bubbles, the calculations overestimate the collapse time by about 20%. Two additional factors in addition to the uncertainty regarding the blood parameters could cause this deviation: (1) the bubbles in the tests are reported to be non-spherical and are attached to a wall; (2) the reported value of the initial radius is not measured directly at the beginning of the experiment but is extrapolated from the measurements at later times. The overall agreement of the data and the simulations shows that the proposed model is capable of predicting the radius–time relations for the dissolving microbubbles.

The collapse time as a function of the initial content of oxygen in blood is shown in Fig. 3. In the simulations, the initial content of oxygen in blood is varied within the physiological conditions with an oxygen partial pressure from 25 to 77 mmHg. For comparison purposes, the calculated time is plotted together with a test computation where the uptake of oxygen is excluded from the model and with the results which are obtained using the Epstein–Plesset model.

In the Epstein–Plesset model, the flux of oxygen from the bubble at a given instance is computed neglecting the movement of the bubble interface at the same instance. In our simulations, the interface movement and the diffusion problem are coupled. Thus, the shrinking of the bubble surface towards its center leads to a decrease of the gradient of dissolved gas at the liquid side of the interface. As a consequence the related slow down of the collapse process is predicted by the present model. The results shown in Fig. 3 indicate that the quasi-steady approach of the Epstein–Plesset model leads to a shorter collapse time compared to the model coupling the calculations of diffusion and radius change. In the test cases with an initial bubble radius 50 and 500 μm, the same 8% difference in the simulated collapse times is observed regardless of the initial concentration of oxygen in blood.

Including the oxygen uptake reaction into the simulations causes a reduction of the collapse time due to the sink term which is incorporated into the facilitated diffusion coefficient. The time decreases by 31% for low initial concentrations of oxygen and by 11% for high concentrations. The impact of the reaction of oxygen binding is higher at a low oxygen concentration due to the lower fraction of oxygen bound to hemoglobin. Thus a higher capacity for the oxygen uptake in the initial phase of the collapse exists.

The curves for different bubbles shown in Fig. 3 are parallel, because the calculated collapse time is proportional to the second power of the initial radius R_0. Such self-similarity can be obtained from the dimensional analysis of the parameters of the problem. The collapse time T_c is a function of the parameters which are treated as the variables of the function:

$$T_c = T_c(c, n, P_{50}, \alpha, \rho_{STP}, \rho_b, P_{O_2}, P_R, D, R_0). \tag{24}$$

The application of the π-theorem with the last three parameters chosen to non-dimensionalize the rest of the variables yields to the following equation:

$$T_c = \frac{R^2}{D}\pi\left(c, n, \frac{P_{50}}{P_R}, \alpha P_R, \frac{\rho_{STP} D}{R^2 P_R}, \frac{\rho_b D}{R^2 P_R}, \frac{P_{O_2}}{P_R}\right), \tag{25}$$

where π is a non-dimensional function with all arguments of the function except the last one being constants. Thus, for a given initial concentration of oxygen in blood, the collapse time is proportional to the square of the initial radius and inversely proportional to the diffusivity coefficient.

Different physiological factors including diseases may affect the ability of blood to diffuse and to bound oxygen. For example, the diffusivity coefficient D decreases with the increase of concentration of hemoglobin in RBC [26], and is highly sensitive to the concentration of albumin in plasma [19]. The physiological variables can also trigger a shift in the saturation curve. An increase of the concentration of dissolved carbon dioxide or temperature requires a higher concentration of oxygen for a given saturation level. On the contrary, a rise in pH concentration promotes the steepness of the saturation curve [19]. The shift of the saturation curve leads to a change of the fitting coefficients in Hill's equation.

The impact of various physiological conditions on the collapse time is illustrated in Fig. 4. The plots show the results of a parametric study where the values of the diffusivity D and the Hill's equation parameter P_{50} were changed within the physiological ranges reported in [19,26]. A shift of the saturation curve causes the collapse time to change by approximately 20%, while the decrease of the diffusivity coefficient results in an almost four times slower dissolution. The collapse time shown in the upper part of Fig. 4 is calculated with a constant incremental change of the diffusivity coefficient. The uneven shift of the corresponding curves points out that the collapse time is inversely proportional to the diffusivity coefficient as it follows from the dimensional analysis of the problem.

The collapse time shown in Figs. 1–4 is calculated assuming that the oxygen pressure in the bubble is atmospheric. If the bubble is introduced into the blood stream in cardiopulmonary bypass or as

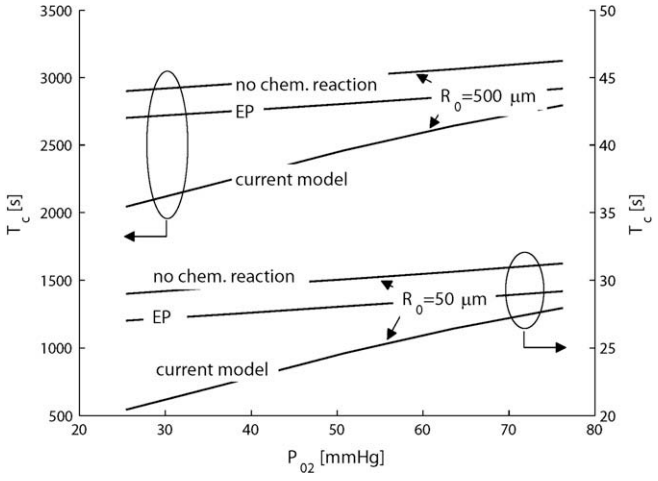

Fig. 3. Collapse time T_c as a function of the initial content of oxygen for two different radii, R_0 = 500 μm (top) and R_0 = 50 μm (bottom); EP denotes the results of the Epstein–Plesset model.

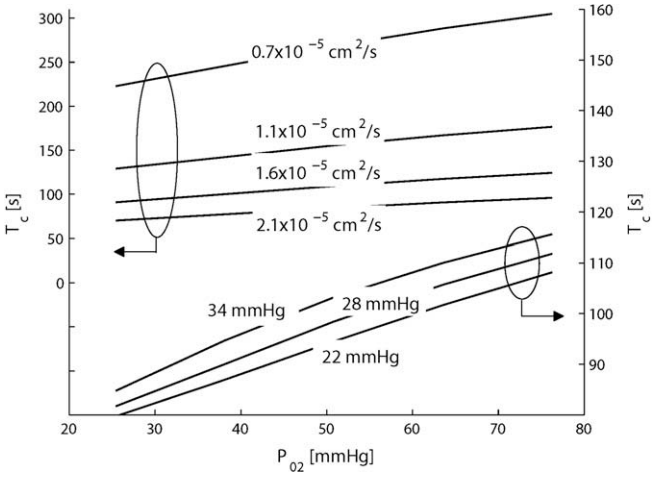

Fig. 4. Collapse time as a function of the initial content of oxygen for different physical conditions. The diffusion coefficient (shown next to curve) is varied between 0.7×10^{-5} cm^2 s^{-1} and 2.1×10^{-5} cm^2 s^{-1} (top). The Hill's parameter P_{50} (shown next to curve) is varied between 34 and 28 mmHg (bottom).

a result of cavitation in an artificial heart, the pressure of oxygen inside the bubble may differ from the atmospheric pressure. In the presented model, the pressure inside the bubble is a free parameter which was varied to estimate the influence of the gas pressure on the collapse time. In Fig. 5, the curves delineate regions of the collapse time for the bubbles with an initial radius of 50 and 500 μm. The data is computed for the values of diffusivity D and the Hill's parameter P_{50} which provide the upper and the lower bounds of the collapse time [19,34]. The simulations show that smaller bubbles with high oxygen pressure should collapse in about 10 s. Larger bubbles with low gas pressure may last in blood for several hours.

In the simulations, the bubble is assumed to be surrounded by a relatively large volume of blood such that the bubble collapses before the dissolved oxygen reaches the outer boundary of the simulated blood volume. The profile of the dissolved oxygen at the collapse moment shown in Fig. 1 indicates that oxygen from a bubble diffuses up to three initial radii from the center of the bubble. If a second bubble with the same initial radius is located at a distance less than six radii from the first bubble, the concentration profile of oxygen should be affected by the interference of the dissolved gas diffused from the different bubbles. The interference should increase the collapse time due to a higher amount of gas that has to be absorbed by the same blood volume.

While the analysis of clusters of bubbles is beyond the scope of the present study, the boundary conditions of the model with a single bubble can be modified to obtain an estimate of the impact of multiple bubbles on the collapse time. If two identical bubbles dissolve simultaneously, the symmetry of the problem implies that the gradient of the concentration of dissolved gas in the midpoint between the two bubble centers equals zero. Consequently the diffusion problem for two bubbles can be solved in the semi-space with Neumann boundary conditions imposed at the plane of symmetry. We conducted series of simulations enforcing zero-gradient conditions at the domain boundary. The calculated collapse time is shown in Fig. 6 for different lengths L_D of the computational domain. The simulations may be interpreted as an approximation of the diffusion problem for a bubble which is surrounded by multiple bubbles of the same size which are equally spaced at the distance $\Delta = 2L_D$ from the center of the bubble.

The radius–time relations shown in Fig. 6 illustrate the increase of the collapse time due to the shielding effect of the bubbles in the cluster. If the distance Δ between the central bubble and the surrounding bubbles decreases below 6 initial radii, the bubble shrinks only by a fraction and then stabilizes.

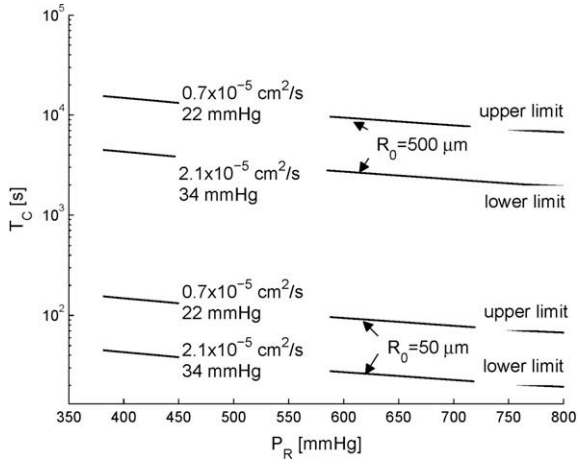

Fig. 5. Collapse time as a function of oxygen pressure inside the bubble P_R for different physiological conditions: diffusivity coefficient and the Hill's parameter P_{50} are shown next to the corresponding curve.

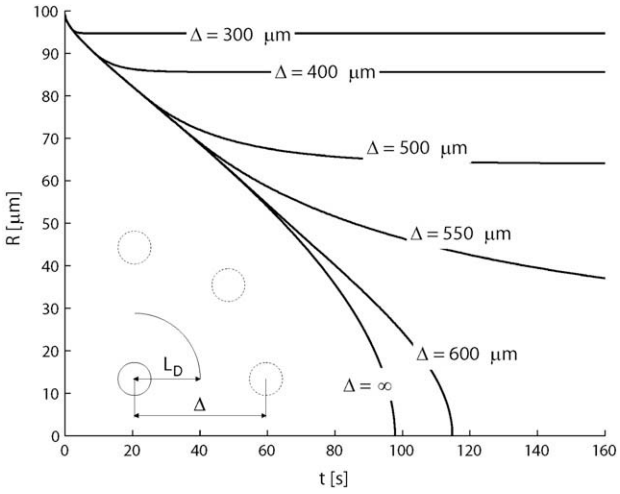

Fig. 6. Radius–time relations for a bubble surrounded by multiple bubbles. The surrounding bubbles are located at distance Δ from the center of the dissolving bubble. The initial radius of the bubbles was set to 100 μm and $D = 1.8 \times 10^{-5}$ cm^2 s^{-1}.

The presence of other bubbles is one of several factors which may affect the accuracy of the prediction of collapse time. To this end, in blood circulation in the human body bubbles take a more elongated shape [2]. The change of the shape may cause more than a 50% increase of the dissolution time as compared with the spherical bubble [1]. When the gas composition is not oxygen, the bubble collapse time may increase as well due to low diffusivity of the mixture components. A layer of denaturated proteins formed at the bubble blood interface results in additional slowdown of the dissolution [1].

At the late stage of the dissolution, the assumption of a constant gas pressure in the bubble has to be revised to take the effect of surface tension into account. Moreover when the bubble radius decreases to approximately 10 μm, the bubble becomes comparable with the size of RBC. In these conditions, the assumption that blood around the bubble can be modeled as a uniform fluid is not acceptable any more.

It could be concluded that the presented model is expected to underestimate the actual life span of the microbubbles in blood. Nevertheless, the computed collapse time may serve as a viable estimate of the lower bound of the dissolution time of single bubbles.

5. Conclusions

The goal of the present work was to simulate the dissolution of oxygen microbubbles in blood. A model has been developed and validated using the radius–time relations reported in the literature for the dissolution of microbubbles.

The results of the simulations have also been used to examine the quasi-steady assumption of the Epstein–Plesset model, which is commonly applied in the analysis of the dissolution of bubbles. The quasi-steady assumption was found to lead to an approximately 8% shorter collapse time as compared to the presented simulations where a fully coupled numerical algorithm was implemented. The simulation of the oxygen uptake reaction results in a reduction of the collapse time of about 30%, as compared to the predictions of the Epstein–Plesset model that neglects chemical reactions.

A parametric study has been conducted to model the dissolution of microbubbles under different physiological conditions. The results showed that the collapse time may vary from 10 s to 2 or 3 h depending on the size of the bubbles and on the parameters which specify the blood conditions.

The limitations of the model have been discussed. It was concluded that the calculated collapse time gives a valuable estimate of the lower bound of the dissolution time of a spherical bubble in blood if the collapse is controlled by the facilitated diffusion of oxygen. Such estimates are useful and alleviate the need for tedious experiments in certain situations.

Appendix A

The concentration at the fictitious node can be evaluated from Eqs. (18) and (19) and the discretized diffusion Eq. (21) as follows:

$$\phi_0 = \frac{-\frac{1}{1+\lambda}\frac{4}{\delta\Delta\eta}\phi_1 + \left(\frac{2}{(1+\lambda)(1+X)} + \frac{dX}{d\tau}\right)\phi_2 + \frac{1}{1+\lambda}\frac{2}{\delta\Delta\eta}\phi_2}{\left(\frac{2}{(1+\lambda)(1+X)} + \frac{dX}{d\tau}\right) - \frac{1}{1+\lambda}\frac{2}{\delta\Delta\eta}}. \tag{26}$$

Substituting Eq. (26) into the expression for the velocity, Eq. (23) yields:

$$\frac{\rho_{STP}}{\rho_b C_0} 6\delta\Delta\eta\left(\frac{dX}{d\tau}\right) = \frac{(-3\phi_1 + 4\phi_2 - \phi_3)\frac{dX}{d\tau} + (-6\phi_1 + 8\phi_2 - 2\phi_3)\frac{1}{(1+\lambda)(1+X)} + (14\phi_1 - 16\phi_2 + 2\phi_3)\frac{1}{(1+\lambda)\delta\Delta\eta}}{\frac{dX}{d\tau} + \frac{2}{(1+\lambda)(1+X)} - \frac{2}{(1+\lambda)\delta\Delta\eta}}. \tag{27}$$

After further simplification one obtains the quadratic equation:

$$\left(\frac{dX}{d\tau}\right)^2 + D\left(\frac{dX}{d\tau}\right) + E = 0, \tag{28}$$

with the coefficients D and E as:

$$D = \frac{2}{1+\lambda}\left(\frac{1}{1+X} - \frac{1}{\delta\Delta\eta}\right) + \frac{\rho_b C_0}{\rho_{STP}}\frac{3\phi_1 - 4\phi_2 + \phi_3}{6\delta\Delta\eta},$$
$$E = \frac{\rho_b C_0}{\rho_{STP}}\frac{1}{3(1+\lambda)\delta\Delta\eta}\left(\frac{3\phi_1 - 4\phi_2 + \phi_3}{1+X} + \frac{-7\phi_1 + 8\phi_2 - \phi_3}{\delta\Delta\eta}\right). \tag{29}$$

The solution of Eq. (28) results in an expression for the velocity of the interface:

$$\left(\frac{dX}{d\tau}\right) = -\frac{1}{2}D - \sqrt{\frac{1}{4}D^2 - E}. \tag{30}$$

References

[1] M. Barak, Y. Katz, Microbubbles – pathophysiology and clinical implications, Chest 128 (2005) 2918–2932.
[2] J.L. Bull, Cardiovascular bubble dynamics, Crit. Rev. Biomed. Eng. 33 (4) (2005) 299–346.
[3] J.R. Street, A.L. Fricke, L.P. Reiss, Dynamics of phase growth in viscous, non-Newtonian liquids, Ind. Eng. Chem. Fund. 10 (1971) 54–64.
[4] R.D. Patel, Bubble growth in viscous Newtonian liquid, Chem. Eng. Sci. 35 (1980) 2356–2358.
[5] D.C. Venerus, N. Yala, Transport analysis of diffusion-induced bubble growth and collapse in viscous liquids, AIChE J. 43 (11) (1997) 2948–2959.
[6] T.A. Shedd, General model for estimating bubble dissolution and droplet evaporation times, J. Microlith. Microfab. Microsyst. 4 (3) (2005) 033004.
[7] V. Pai, M. Favelukis, Dynamics of spherical bubble growth, J. Cell. Plast. 38 (5) (2002) 403–419.
[8] K. Taki, Experimental and numerical studies on the effects of pressure release rate on number density of bubbles and bubble growth in a polymeric foaming process, Chem. Eng. Sci. 63 (2008) 3643–3653.
[9] I. Tanasawa, D.R. Wotton, W.J. Yang, D.W. Clark, Experimental study of air bubbles in a simulated cardiopulmonary bypass system with flow constriction, J. Biomech. 3 (1970) 417–424.
[10] H.D. Van Liew, M.E. Burkard, Bubbles in circulating blood: stabilization and simulations of cyclic changes of size and content, J. Appl. Physiol. 79 (1995) 1379–1385.
[11] E.A. Brujan, Collapse of cavitation bubbles in blood, Europhys. Lett. 50 (2) (2000) 175–181.
[12] A.J. Reddy, A.J. Szeri, Coupled dynamics of translation and collapse of acoustically driven microbubbles, J. Acoust. Soc. Am. 112 (4) (2002) 1346–1352.
[13] C.A. MacDonald, V. Sboros, J. Gomatam, S.D. Pye, C.M. Moran, W.N. McDicken, A numerical investigation of the resonance of gas-filled microbubbles: resonance dependence on acoustic pressure amplitude, Ultrasonics 43 (2004) 113–122.
[14] J.I. Iloreta, Y. Zhou, G.N. Sankin, P. Zhong, A.J. Szeri, Assessment of shock wave lithotripters via cavitation potential, Phys. Fluids 19 (2007) 086103.
[15] P.S. Epstein, M.S. Plesset, On the stability of gas bubbles in liquid–gas solutions, J. Chem. Phys. 18 (11) (1950) 1505–1509.
[16] A. Kabalnov, D. Klein, T. Pelura, E. Schutt, J. Weers, Dissolution of multicomponent microbubbles in the bloodstream: 1. Theory, Ultrasound Med. Biol. 24 (5) (1998) 739–749.
[17] E. Rambod, M. Beizaie, M. Shusser, S. Milo, M. Gharib, A physical model describing the mechanism for formation of gas microbubbles in patients with mitral mechanical heart valves, Ann. Biomed. Eng. 27 (1999) 774–792.
[18] O.D. Kripfgans, J.B. Fowlkes, D.L. Miller, O.P. Eldevik, P.L. Carson, Acoustic droplet vaporization for therapeutic and diagnostic applications, Ultrasound Med. Biol. 26 (7) (2000) 1177–1189.
[19] T.K. Goldstick, Oxygen transport, in: J.H.V. Brown, D.S. Gann (Eds.), Engineering Principles in Physiology, vol. 2, Academic Press, New York, 1973, pp. 257–283.
[20] J.H. Meldon, Blood–gas equilibria, kinetics and transport, Chem. Eng. Sci. 42 (2) (1987) 199–211.
[21] W.J. Yang, Dynamics of gas bubbles in whole blood and plasma, J. Biomech. 4 (2) (1971) 119–125.
[22] W.J. Yang, R. Echigo, D.R. Wotton, J.B. Hwang, Experimental studies of the dissolution of gas bubbles in whole blood and plasma-I. Stationary bubbles, J. Biomech. 4 (1971) 228–275.
[23] W.J. Yang, R. Echigo, D.R. Wotton, J.W. Ou, J.B. Hwang, Mass transfer from gas bubbles to impinging flow of biological fluids with chemical reaction, Biophys. J. 12 (11) (1972) 1391–1404.
[24] R.S. Srinivasan, W.A. Gerth, M.R. Powell, Mathematical models of diffusion-limited gas bubble dynamics in tissue, J. Appl. Physiol. 86 (1999) 732–741.
[25] J.T. Coin, J.S. Olson, The rate of oxygen uptake by human red blood cells, J. Biol. Chem. 254 (4) (1979) 1178–1190.
[26] K.D. Vandegriff, J.S. Olson, Morphological and physiological factors affecting oxygen uptake and release by red blood cells, J. Biol. Chem. 259 (20) (1984) 12619–12627.
[27] K. Yamaguchi, D. Nguyen-Phu, P. Scheid, J. Piipe, Kinetics of O_2 uptake and release by human erythrocytes studied by a stopped-flow technique, J. Appl. Physiol. 58 (4) (1985) 1215–1224.
[28] E. Heidelberger, R.B. Reeves, O_2 transfer kinetics in a whole blood unicellular thin layer, J. Appl. Physiol. 68 (5) (1990) 1854–1864.
[29] S.T. Bouwer, L. Hoofd, F. Kreuzer, Reaction rates of oxygen with hemoglobin measured by non-equilibrium facilitated oxygen diffusion through hemoglobin solutions, Biochim. Biophys. Acta 1525 (2001) 108–117.
[30] D.M. Eckmann, J. Zhang, J. Lampe, P.S. Ayyaswamy, Gas embolism and surfactant-based intervention. Implications for long-duration space-based activity, Ann. NY Acad. Sci. 1077 (2006) 256–269.
[31] I. Kutschka, U. Schönrock, A. El Essawi, D. Pahari, M. Anssar, W. Harringer, A new minimized perfusion circuit provides highly effective ultrasound controlled deairing, Artif. Organs 31 (3) (2007) 215–220.
[32] J.D. Goddard, Further applications of carrier-mediated transport theory – a survey, Chem. Eng. Sci. 32 (1977) 795–809.
[33] E. Pecou, Splitting the dynamics of large biochemical interaction networks, J. Theor. Biol. 232 (3) (2005) 375–384.
[34] J.D. Bronzino, The Biomedical Engineering Handbook, third ed., CRC Press, 2006.
[35] S.N. Vaslef, R.W. Anderson, R.J. Leonard, Use of a mathematical model to predict oxygen transfer rates in hollow fiber membrane oxygenators, ASAIO J. 40 (4) (1994) 990–996.
[36] T.J. Hewitt, B.G. Hattler, W.J. Federspiel, A mathematical model of gas exchange in an intravenous membrane oxygenator, Ann. Biomed. Eng. 26 (1998) 166–178.
[37] J. Zhang, T.C. Nolan, T. Zhang, B.P. Griffith, Z.J. Wu, Characterization of membrane blood oxygenation devices using computational fluid dynamics, J. Membr. Sci. 288 (2007) 268–279.
[38] M. Fischer, M. Dietzel, D. Poulikakos, Thermally enhanced solubility for the shrinking of a nanoink droplet in a surrounding liquid, Int. J. Heat Mass Transfer 52 (2009) 222–231.
[39] H.G. Landau, Heat conduction in a melting solid, Q. Appl. Math. 8 (1950) 81–94.
[40] J.H. Ferziger, M. Peric, Computational Methods for Fluid Dynamics, third ed., Springer, New York, 2002. p. 44.